Topological $\mathbb{Z}_2$ resonating-valence-bond spin liquid on the square lattice

Ji-Yao Chen and Didier Poilblanc

Laboratoire de Physique Théorique, C. N. R. S. and Université de Toulouse, 31062 Toulouse, France

A one-parameter family of long-range resonating-valence-bond (RVB) state on the square lattice was previously proposed to describe a critical spin liquid (SL) phase of the spin-1/2 frustrated Heisenberg model. We provide evidence that this RVB state in fact also realizes a topological (long-range entangled) $\mathbb{Z}_2$ SL, limited by two transitions to critical SL phases. The topological phase is naturally connected to the $\mathbb{Z}_2$ gauge symmetry of the local tensor. This Rapid Communication shows that, on one hand, spin-1/2 topological SL with C_{4v} point-group symmetry and $SU(2)$ spin rotation symmetry exists on the square lattice and, on the other hand, criticality and nonbipartiteness are compatible. We also point out that strong similarities between our phase diagram and the ones of classical interacting dimer models suggest both can be described by similar Kosterlitz-Thouless transitions. This scenario is further supported by the analysis of the one-dimensional boundary state. Forms of parent Hamiltonians hosting the $\mathbb{Z}_2$ SL are suggested.

Introduction. In pioneering work [1], Anderson proposed the resonating-valence-bond (RVB) state [2] as the parent Mott insulator for high-temperature superconductivity [3]. In contrast to magnetic phases, the insulating RVB state hosts preexisting (resonating) singlet pairs of spins 1/2—or valence bonds (VBs)—which, upon hole doping, give rise to superconducting (coherent) Cooper pairs. Originally, the RVB state, in its simplest version only involves resonating singlets build from nearest-neighbor (NN) spins 1/2. More recently, a generalized RVB state including longe-range singlet pairs has been introduced to describe the ground state of the spin-1/2 frustrated Heisenberg antiferromagnet on the square lattice [4,5].

In recent years, the notion of topological order [6,7] has progressively emerged as a key concept going beyond the traditional Ginzburg-Landau paradigm of spontaneous symmetry breaking [8,9]. It is at the heart of the excitement for quantum computing as can be conceptually realized in Kitaev's toric code (TC) [10]. Rokhsar-Kivelson (RK) quantum dimer models [11,12] on the kagome and triangular lattices turned out to host dimer liquid phases of the same $\mathbb{Z}_2$ (i.e., Ising) topological class as the TC [13,14]. The kagome NN RVB state also provides a beautiful example—and maybe the simplest possible—of a $\mathbb{Z}_2$ spin liquid (SL) [15–18], the spin-1/2 $SU(2)$-symmetric analog of the RK dimer liquids. Topological order is associated to long-range entanglement providing the roots for the emergence of exotic fractionalized bulk excitations. E.g., the kagome NN RVB state hosts mobile spin-1/2 (electriclike) spinon and spinless (magneticlike) vison excitations [16].

Strikingly, NN RVB states turn out to have very different infrared (i.e., long-distance) properties depending on the bipartiteness or nonbipartiteness of the lattice [16]. For example, in contrast to its analog on the kagome lattice, the NN RVB state on the square lattice exhibits algebraic (dimer-dimer) correlations [19,20]. All spin-1/2 NN RVB states are in fact closely related to their RK dimer-liquid analogs [11]. On the square lattice, a height field representation can be drawn enabling to construct a coarse-grained field theory [21,22] hosting a stable critical Kosterlitz-Thouless (KT) phase. The nonorthogonality of the valence-bond configurations of the NN RVB state does not affect the critical nature of the state but only modifies the critical exponent [19,20,23]. In this Rapid Communication, we show that introducing long-range bonds into the (square lattice) NN RVB state—breaking its bipartiteness nature—leads to a rich phase diagram, including a new topological $\mathbb{Z}_2$ SL, bounded by two critical KT phases.

The RVB as a simple projected entangled-pair state. For this goal, we consider the generalized RVB state on the square lattice, which was introduced in Ref. [4]. Such a state is represented as a simple projected entangled-pair state (PEPS) which, after applying a π rotation along the Y-spin axis on one of the two sublattices, only involves a single tensor $\mathcal{A}$ on every site. The tensor $\mathcal{A}$ is obtained by linear combining two $\mathcal{A}_1$ tensors, both of which belong to the A_1 irreducible representation of the square lattice point-group C_{4v}:

$$\mathcal{A} = \mathcal{A}_1^{(1)} + \lambda \mathcal{A}_1^{(2)}. \tag{1}$$

The $\mathcal{A}_1^{(1)}$ ($\mathcal{A}_1^{(2)}$) tensor has one (three) virtual spin-1/2 and three (one) virtual spin-0 in every site configuration and correspondingly one (three) virtual dimer(s) attached to every lattice site. Virtual spin-1/2 on the bonds connecting NN sites are paired up into singlets. The four virtual spins attached to every site are then projected into the physical spin-1/2. The bond dimension is thus $D = 3$. The elements of $\mathcal{A}_1^{(1,2)}$ which can be found in Ref. [24] are reproduced in the Supplemental Material [25] for convenience and graphically represented in Figs. 1(a) and 1(b). The PEPS formed by $\mathcal{A}_1^{(1)}$ is exactly the bosonic equal weight NN RVB state [26], and adding the $\mathcal{A}_1^{(2)}$ tensor will generate longer-range VB through quantum teleportation
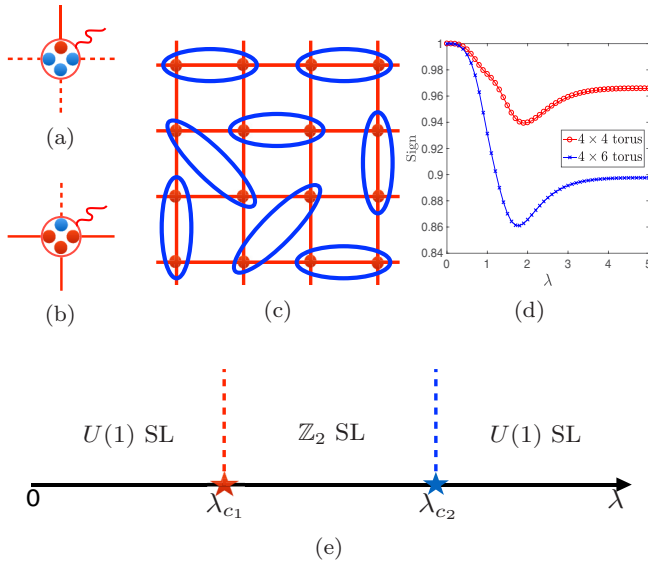
FIG. 1. (a, b) Schematic representations of the $\mathcal{A}_1^{(1)}$ and $\mathcal{A}_1^{(2)}$ site tensors, respectively. The red (blue) dots represent virtual spins 1/2 (0), the solid (dotted) lines represent virtual dimers (absence of dimers), and the red circle stands for the projection operator. The other tensor elements are obtained by rotation and reflection symmetries. (c) Typical VB configuration on the square lattice where ellipses stand for singlet pairs of spin-1/2. (d) Marshall sign versus λ. (e) Phase diagram of the PEPS given by Eq. (1) versus λ.

[4]. The violation of the Marshall sign [see Fig. 1(d) and discussion below] implies that singlet VB can appear within the same sublattice, meaning that, strictly speaking, bipartiteness is broken once $\lambda \neq 0$. A typical VB configuration is shown in Fig. 1(c). Since in every VB configuration the number of $\mathcal{A}_1^{(2)}$ tensor is even, $\mathcal{A}(\lambda)$ and $\mathcal{A}(-\lambda)$ represent the same state, and one can restrict to, e.g., $\lambda \geqslant 0$.

To draw a phase diagram as a function of the parameter λ, we have used a corner transfer matrix renormalization group (CTMRG) method [27–29] taking advantage of the tensor symmetries [5] to compute the spin and dimer correlation functions. This has been supplemented by a tensor renormalization group (TRG) analysis to extract topological properties, if any. Our results are summarized in the schematic phase diagram shown in Fig. 1(e). A short-range topological $\mathbb{Z}_2$ SL phase is found in an extended region $\lambda \in (\lambda_{c_1}, \lambda_{c_2})$, surrounded by two critical SL phases, where $\lambda_{c_1} = 0.85(5)$, $\lambda_{c_2} = 2.85(5)$. We emphasize the existence of an emergent $U(1)$ gauge field responsible for the critical nature of the SL phases at $\lambda < \lambda_{c_1}$ and $\lambda > \lambda_{c_2}$. Next, we present our numerical results supporting this phase diagram.

Marshall sign and gauge symmetry. The PEPS we are considering is a $SU(2)$ spin singlet and can be expressed as coherent superposition of valence-bond configurations, which form an overcomplete basis:

$$|\psi(\mathcal{A})\rangle = \sum c_{(i_1 j_1),(i_2 j_2),\ldots} |(i_1 j_1),(i_2 j_2),\ldots\rangle, \quad (2)$$

where $|(i_1 j_1),(i_2 j_2),\ldots\rangle$ is a VB configuration and $c_{(i_1 j_1),(i_2 j_2),\ldots}$ is the corresponding amplitude. Note that, in general we cannot

factorize $c_{(i_1 j_1),(i_2 j_2),\ldots}$ as a product of weights function of the dimer length. A central question to ask is what is the (ij) singlet pairing type in the VB basis, i.e., whether there is only inter-sublattice AB pairing. To answer this question, we have investigated the Marshall sign [30] in the Ising basis. We put the PEPS on a finite lattice with torus geometry and use exact contraction to obtain the wave function. Then we compute the Marshall sign average, defined as $\langle \text{sign} \rangle = \frac{\sum_c \text{sgn}_c |\langle c|\psi(\mathcal{A})\rangle|^2}{\sum_c |\langle c|\psi(\mathcal{A})\rangle|^2}$, where c is the Ising configuration and sgn_c is determined by the sign of the coefficient. As can be seen in Fig. 1(d), for arbitrarily small $\lambda \neq 0$, the Marshall sign average deviates from 1 and more severely with increasing system size. These results imply that our RVB PEPS cannot be written in the canonical Liang-Douçot-Anderson form [31] with only (AB) singlet pairs. Reversely, if VBs are present on the same A or B sublattices, it implies that, effectively, the bipartiteness of the lattice is broken. This property is in fact connected to the broken $U(1)$ gauge symmetry of the site tensor: For $\lambda = 0$ ($\lambda = \infty$) the number of virtual spin-1/2 around each site is fixed to 1 (3), whereas for $0 < \lambda < \infty$, only the *parity* of this number is conserved so that the $U(1)$ gauge symmetry is broken down to $\mathbb{Z}_2$. The two $U(1)$-symmetric RVB states are in fact closely related to their RK critical dimer-liquid analogs [11] for which the KT algebraic (dimer) correlations follow from a coarse-grained height-field theory [21,22]. At finite λ, the long-distance field theory can no longer be obtained by the same coarse-graining procedure. Therefore, it is not clear whether each algebraic phase will survive in a finite region of the parameter λ. Next, we provide numerical evidence for the stability of both critical phases and the emergence of a novel short-range SL in between.

Correlation functions. To calculate the physical observables of the PEPS given by Eq. (1), we use the CTMRG method to extract various correlation functions [5,27–29]. The CTMRG method allows us to work directly in the thermodynamic limit, whose accuracy is controlled by the bond dimension of environment tensors, denoted as χ. For completeness, we include the details of the specific CTMRG method we are using in the Supplemental Material [25]. We are interested in spin-spin and longitudinal/transverse dimer-dimer correlation functions along, e.g., the $\mathbf{e}_x$ (horizontal) direction defined as:

$$
\begin{aligned}
C_s(d) &= \langle \mathbf{S_i} \cdot \mathbf{S_{i+d e_x}} \rangle_0, \\
C_d^{(L)}(d) &= \langle D_{\mathbf{i}}^x D_{\mathbf{i}+d\mathbf{e}_x}^x \rangle_0 - \langle D_{\mathbf{i}}^x \rangle_0 \langle D_{\mathbf{i}+d\mathbf{e}_x}^x \rangle_0, \\
C_d^{(T)}(d) &= \langle D_{\mathbf{i}}^y D_{\mathbf{i}+d\mathbf{e}_x}^y \rangle_0 - \langle D_{\mathbf{i}}^y \rangle_0 \langle D_{\mathbf{i}+d\mathbf{e}_x}^y \rangle_0, \quad (3)
\end{aligned}
$$

where the dimer operators $D_{\mathbf{i}}^x = \mathbf{S_i} \cdot \mathbf{S_{i+e_x}}$ and $D_{\mathbf{i}}^y = \mathbf{S_i} \cdot \mathbf{S_{i+e_y}}$. Note that the correlation along the $\mathbf{e}_y$ (vertical) direction is the same due to C_{4v} lattice symmetry. Also, since L and T dimer correlations give similar results, we will only show the T correlations for conciseness.

The spin-spin correlations show clear exponential decay with momentum (π, π) in all parameter region. Typical behaviors for $\chi = 12D^2$ are shown in Fig. 2(a). By fitting the asymptotic linear behaviors of the data according to $\ln |C_s(d)| = -(1/\xi_s)d + c_0$, we straightforwardly get the correlation length
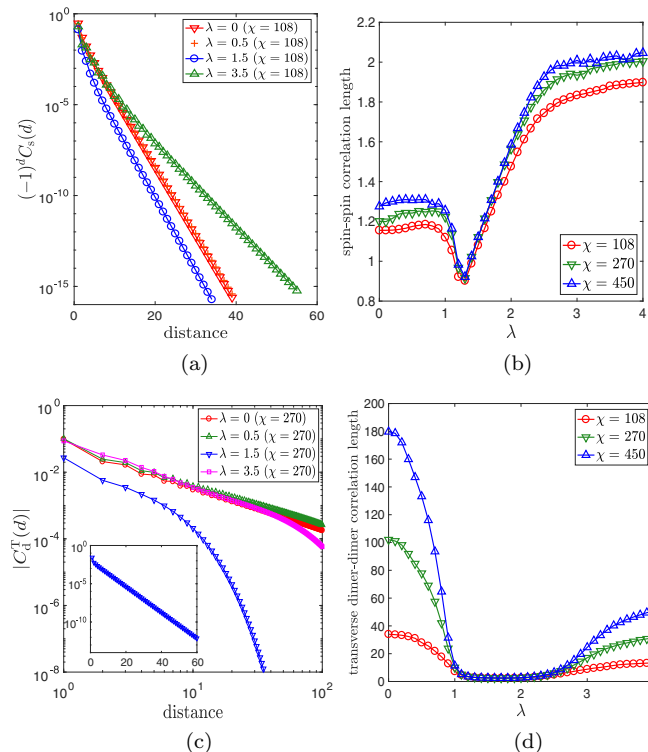
FIG. 2. (a) Spin correlation function versus distance for different λ's at fixed $\chi = 12D^2$ (semi-log plot). (b) Spin correlation length versus λ for different values of χ. (c) Log-log plot of the (transverse) dimer correlation versus distance for different λ's at fixed $\chi = 30D^2$ (semi-log plot for $\lambda = 1.5$ in the inset). (d) Dimer correlation length versus λ for different values of χ [same as in (b)]. In (b) and (d) the error bar of fitting correlation length is smaller than symbol size and has been omitted.

FIG. 3. (a) Dimer (transverse) correlation length versus χ/D^2 for different values of λ. (b) Fits versus D^2/χ of the exponent of the power-law dimer correlation, for different values of λ in the critical phases. (c) and (d) Dimer exponent versus λ for different values of χ and $\chi \to \infty$ extrapolation. In (b)–(d), the error bar of the exponent at finite χ comes from fitting the dimer correlation functions versus distance, whereas the error bar of the extrapolated exponent comes from linear fitting versus D^2/χ.

ξ_s from the slopes $-1/\xi_s$, which is shown in Fig. 2(b). It can be seen that the spin-spin correlation length is very short in the full parameter region and, with increasing χ, converges to a small finite value. Note however that a small singularity may be present around $\lambda \simeq 0.9$, reflecting some transition (see next).

The dimer-dimer correlations reveal new exotic features. For both small λ ($\lambda < \lambda_{c_1}$) and large λ ($\lambda > \lambda_{c_2}$), the analysis of the data shows clear power-law decaying dimer-dimer correlations as can be seen, e.g., in Fig. 2(c). Although for any finite χ, the asymptotic long-distance dimer-dimer correlations decay always exponentially, the correlation length ξ_d [see Fig. 2(d)] never saturates with increasing χ as can be seen in Fig. 3(a), which indicates that the two regions are in fact critical. By fitting the critical behavior $|C_d(d)| \sim d^{-\eta}$ in the $d \leqslant \xi_d$ region, we can obtain the critical exponent η, shown in Figs. 3(b)–3(d). The converged exponent at $\lambda = 0$ (NN RVB state) agrees very well with Monte Carlo results [19,20]. By analyzing the behavior of the dimer correlation length with increasing χ, we have located the phase boundaries $\lambda_{c_1} = 0.85(5)$, $\lambda_{c_2} = 2.85(5)$. Most strikingly, in the intermediate $\lambda_{c_1} < \lambda < \lambda_{c_2}$ region, $\xi_d(\chi)$ clearly saturates to a small value, as shown in Fig. 2(d), revealing a true short-range behavior.

Search for topological order. The exponentially decaying spin and dimer correlation functions (with extremely short correlation leng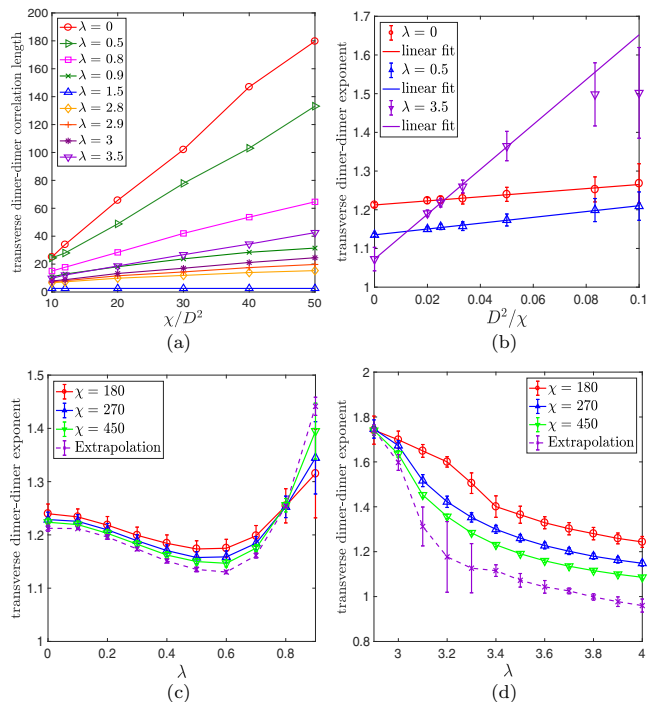ths) strongly support the existence of a new quantum phase between λ_{c_1} and λ_{c_2}. Furthermore, since there is no evidence for any symmetry-breaking order, it should be a short-range spin liquid. Then, a natural question is whether this spin liquid exhibits topological order. The PEPS in Eq. (1) bears $\mathbb{Z}_2$ gauge symmetry, except at $\lambda = 0, \infty$ where higher $U(1)$ gauge symmetry is present. The $\mathbb{Z}_2$ gauge symmetry is generated by 2π spin rotation, which only induces a minus sign in the $\mathcal{A}$ tensor. We then expect $\mathbb{Z}_2$ topological order in the intermediate region. To verify this, we use the TRG method to obtain the modular matrices. Note that, in order to correctly implement this method, we need to keep the $\mathbb{Z}_2$ gauge symmetry [32,33]. The TRG method for modular matrices is briefly reviewed in the Supplemental Material [25], whose precision is controlled by the bond dimension χ of the double tensor. After every TRG step, we put the double tensor on a torus. Inserting gauge symmetry transformation, we obtain the complete modular S and T matrices. In the intermediate region, the modular matrices converge after six TRG steps, whereas it takes much longer (typically 10–12 steps) to obtain converged results in the critical regions, as shown in Fig. 4(a).

The converged modular matrices for the short-range SL are as follows:

$$S = \begin{pmatrix} 1 & 0 & 0 & 0 \\ 0 & 0 & 1 & 0 \\ 0 & 1 & 0 & 0 \\ 0 & 0 & 0 & 1 \end{pmatrix}, \quad T = \begin{pmatrix} 1 & 0 & 0 & 0 \\ 0 & 1 & 0 & 0 \\ 0 & 0 & 0 & 1 \\ 0 & 0 & 1 & 0 \end{pmatrix}, \quad (4)$$
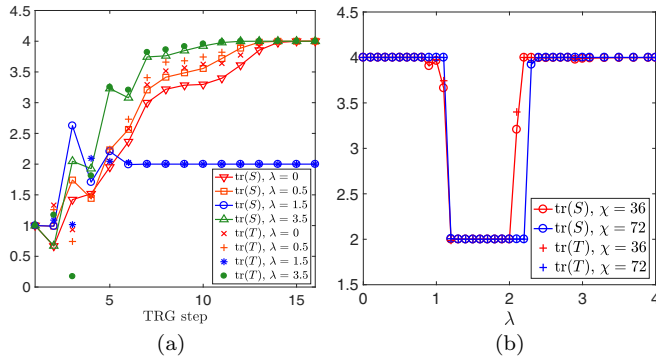
FIG. 4. Trace of the modular matrices S and T. (a) versus TRG step number at $\chi = 8D^2$; (b) versus λ after 12 and 16 steps at $\chi = 4D^2$ and $8D^2$, respectively.
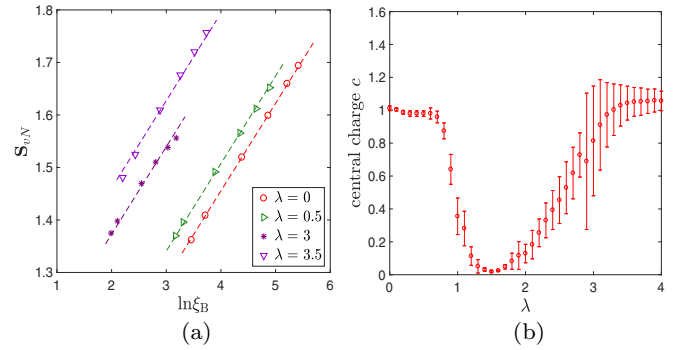

FIG. 5. (a) von Neumann entropy versus the logarithm of the maximal correlation length. The dashed lines correspond to CFT predictions with $c = 1$. (b) Central charge c from linear fits of the data. Note, in the second critical phase, data with $\chi \geqslant 20D^2$ only are used in the fit.

which are identical to the modular matrices of the TC in the string basis. For the two critical regions, we also obtain converged modular matrices:

$$S = \begin{pmatrix} 1 & 1 & 1 & 1 \\ 1 & 1 & 1 & 1 \\ 1 & 1 & 1 & 1 \\ 1 & 1 & 1 & 1 \end{pmatrix}, \quad T = \begin{pmatrix} 1 & 1 & 1 & 1 \\ 1 & 1 & 1 & 1 \\ 1 & 1 & 1 & 1 \\ 1 & 1 & 1 & 1 \end{pmatrix}, \quad (5)$$

which are rank-1 matrices and indicate trivial topological order. The trace of the converged modular matrices for different λ's is shown in Fig. 4(b) where sharp transitions can be seen between the different regions. We note that, similar topological information can also be obtained by investigating the leading eigenvalues of the transfer matrix in different topological sectors when putting the PEPS on an infinitely long cylinder [34].

Boundary conformal field theory for $U(1)$ SL. The existence of the two critical SL phases (beyond the $\lambda = 0$ and $\lambda = \infty$ points) is further supported by the analysis of the boundary state (see the Supplemental Material [25] for details). We find that the corresponding von Neumann entanglement entropy scales with the maximal correlation length ξ_B of the boundary state when increasing χ, like $\mathbf{S}_{vN}(\chi) \sim \frac{c}{6} \ln \xi_B(\chi)$, as expected in a $(1+1)$-dimensional conformal field theory (CFT) with universal central charge c [35,36]. From the fits of Fig. 5, one gets $c = 1.01(2)$ and $c = 1.05(6)$, consistent with a simple $c = 1$ CFT.

Conclusion and outlook. Using a simple PEPS ansatz of a generalized RVB spin liquid, we have shown that: (i) spin-$1/2$ topological SL with C_{4v} point-group symmetry and $SU(2)$-spin rotation symmetry exists on the square lattice and (ii) criticality and nonbipartiteness are compatible. The topological phase observed here is naturally connected to the

$\mathbb{Z}_2$ gauge symmetry of the local tensor typical of an Ising gauge theory [12,22]. These properties are reminiscent of a classical interacting dimer model which interpolates between the square lattice and the triangular lattice by tuning a chemical potential in the diagonal bonds [37]. In this case, by varying the temperature, a similar transition is seen separating a high-temperature short-range disordered dimer liquid to a critical KT low-temperature dimer phase. In fact, the NN RVB phase can be mapped to a classical *interacting* dimer model on the square lattice at finite temperature [23,38,39]. Although it is not clear how such a mapping could be extended once $\lambda \neq 0$, the similarity between the two phase diagrams suggests that both can be captured by the same long-wavelength height-field theory [37,39,40], giving rise to (continuous) KT phase transitions. Such a scenario is supported by the finding of a universal boundary central charge $c = 1$ in the two critical regions.

Finally, we note that the existence of a $SU(2)$-invariant *local* parent Hamiltonian follows from the $\mathbb{Z}_2$ injectivity of the PEPS [15]. The latter at $\lambda \neq 0$ would be a "deformation" of the parent Hamiltonian derived at $\lambda = 0$ (see the Supplemental Material and Refs. [41,42]), including, e.g. (physically relevant) plaquette cyclic terms or other sorts of multi-spin interactions involving up to six sites.

[1] P. W. Anderson, The resonating valence bond state in La$_2$CuO$_4$ and superconductivity, Science **235**, 1196 (1987).

[2] P. Fazekas and P. W. Anderson, On the ground state properties of the anisotropic triangular antiferromagnet, Philos. Mag. **30**, 423 (1974).

[3] J. G. Bednorz and K. A. Müller, Possible high T$_c$ superconductivity in the BaLaCuO system, Z. Phys. B **64**, 189 (1986).

[4] L. Wang, D. Poilblanc, Z.-C. Gu, X.-G. Wen, and F. Verstraete, Constructing a Gapless Spin-Liquid State for the Spin-$1/2$ $J_1 - J_2$ Heisenberg Model on a Square Lattice, Phys. Rev. Lett. **111**, 037202 (2013).

[5] D. Poilblanc and M. Mambrini, Quantum critical phase with infinite projected entangled paired states, Phys. Rev. B **96**, 014414 (2017).

[6] X. G. Wen, Topological orders in rigid states, Int. J. Mod. Phys. B **04**, 239 (1990).

[7] X.-G. Wen, Topological order: From long-range entangled quantum matter to a unified origin of light and electrons, ISRN Condens. Matter Phys. **2013**, 198710 (2013).

[8] L. D. Landau, Zur Theorie der phasenumwandlungen II, Phys. Z. Sowjetunion **11**, 26 (1937).

[9] V. L. Ginzburg and L. D. Landau, On the Theory of superconductivity, Zh. Eksp. Teor. Fiz. **20**, 1064 (1950).

[10] A. Y. Kitaev, Fault-tolerant quantum computation by anyons, Ann. Phys. (NY) **303**, 2 (2003).

[11] D. S. Rokhsar and S. A. Kivelson, Superconductivity and the Quantum Hard-Core Dimer Gas, Phys. Rev. Lett. **61**, 2376 (1988).

[12] R. Moessner, S. L. Sondhi, and E. Fradkin, Short-ranged resonating valence bond physics, quantum dimer models, and Ising gauge theories, Phys. Rev. B **65**, 024504 (2001).

[13] G. Misguich, D. Serban, and V. Pasquier, Quantum Dimer Model on the Kagome Lattice: Solvable Dimer-Liquid and Ising Gauge Theory, Phys. Rev. Lett. **89**, 137202 (2002).

[14] A. Ralko, M. Ferrero, F. Becca, D. Ivanov, and F. Mila, Zero-temperature properties of the quantum dimer model on the triangular lattice, Phys. Rev. B **71**, 224109 (2005).

[15] N. Schuch, D. Poilblanc, J. I. Cirac, and D. Pérez-García, Resonating valence bond states in the peps formalism, Phys. Rev. B **86**, 115108 (2012).

[16] D. Poilblanc, N. Schuch, D. Pérez-García, and J. I. Cirac, Topological and entanglement properties of resonating valence bond wave functions, Phys. Rev. B **86**, 014404 (2012).

[17] J. Wildeboer and A. Seidel, Correlation Functions in SU(2)-Invariant Resonating-Valence-Bond Spin Liquids on Nonbipartite Lattices, Phys. Rev. Lett. **109**, 147208 (2012).

[18] F. Yang and H. Yao, Frustrated Resonating Valence Bond States in two Dimensions: Classification and Short-Range Correlations, Phys. Rev. Lett. **109**, 147209 (2012).

[19] A. F. Albuquerque and F. Alet, Critical correlations for short-range valence-bond wave functions on the square lattice, Phys. Rev. B **82**, 180408 (2010).

[20] Y. Tang, A. W. Sandvik, and C. L. Henley, Properties of resonating-valence-bond spin liquids and critical dimer models, Phys. Rev. B **84**, 174427 (2011).

[21] E. Fradkin and S. Kivelson, Short range resonating valence bond theories and superconductivity, Mod. Phys. Lett. B **04**, 225 (1990).

[22] E. Fradkin, *Field Theories of Condensed Matter Physics*, 2nd ed. (Cambridge University Press, Cambridge, 2013) .

[23] K. Damle, D. Dhar, and K. Ramola, Resonating Valence Bond Wave Functions and Classical Interacting Dimer Models, Phys. Rev. Lett. **108**, 247216 (2012).

[24] M. Mambrini, R. Orús, and D. Poilblanc, Systematic construction of spin liquids on the square lattice from tensor networks with SU(2) symmetry, Phys. Rev. B **94**, 205124 (2016).

[25] See Supplemental Material at http://link.aps.org/supplemental/10.1103/PhysRevB.97.161107 for a list of the nonzero elements of the tensors $\mathcal{A}_1^{(1,2)}$, CTMRG method for correlation functions, and the TRG method for modular matrices. We also define and

[26] F. Verstraete, M. M. Wolf, D. Perez-Garcia, and J. I. Cirac, Criticality, the Area Law, and the Computational Power of Projected Entangled Pair States, Phys. Rev. Lett. **96**, 220601 (2006).

[27] T. Nishino and K. Okunishi, Corner transfer matrix renormalization group method, J. Phys. Soc. Jpn. **65**, 891 (1996).

[28] R. Orús and G. Vidal, Simulation of two-dimensional quantum systems on an infinite lattice revisited: Corner transfer matrix for tensor contraction, Phys. Rev. B **80**, 094403 (2009).

[29] R. Orús, Exploring corner transfer matrices and corner tensors for the classical simulation of quantum lattice systems, Phys. Rev. B **85**, 205117 (2012).

[30] W. Marshall, Antiferromagnetism, Proc. R. Soc. London, Ser. A **232**, 48 (1955).

[31] S. Liang, B. Doucot, and P. W. Anderson, Some New Variational Resonating-Valence-Bond-Type Wave Functions for the Spin-$\frac{1}{2}$ Antiferromagnetic Heisenberg Model on a Square Lattice, Phys. Rev. Lett. **61**, 365 (1988).

[32] H. He, H. Moradi, and X.-G. Wen, Modular matrices as topological order parameter by a gauge-symmetry-preserved tensor renormalization approach, Phys. Rev. B **90**, 205114 (2014).

[33] J.-W. Mei, J.-Y. Chen, H. He, and X.-G. Wen, Gapped spin liquid with $\mathbb{Z}_2$ topological order for the kagome heisenberg model, Phys. Rev. B **95**, 235107 (2017).

[34] N. Schuch, D. Poilblanc, J. I. Cirac, and D. Pérez-García, Topological Order in the Projected Entangled-Pair States Formalism: Transfer Operator and Boundary Hamiltonians, Phys. Rev. Lett. **111**, 090501 (2013).

[35] F. Pollmann, S. Mukerjee, A. M. Turner, and J. E. Moore, Theory of Finite-Entanglement Scaling at One-Dimensional Quantum Critical Points, Phys. Rev. Lett. **102**, 255701 (2009).

[36] J. A. Kjäll, M. P. Zaletel, R. S. K. Mong, J. H. Bardarson, and F. Pollmann, Phase diagram of the anisotropic spin-2 xxz model: Infinite-system density matrix renormalization group study, Phys. Rev. B **87**, 235106 (2013).

[37] F. Trousselet, P. Pujol, F. Alet, and D. Poilblanc, Criticality of a classical dimer model on the triangular lattice, Phys. Rev. E **76**, 041125 (2007).

[38] F. Alet, J. L. Jacobsen, G. Misguich, V. Pasquier, F. Mila, and M. Troyer, Interacting Classical Dimers on the Square Lattice, Phys. Rev. Lett. **94**, 235702 (2005).

[39] F. Alet, Y. Ikhlef, J. L. Jacobsen, G. Misguich, and V. Pasquier, Classical dimers with aligning interactions on the square lattice, Phys. Rev. E **74**, 041124 (2006).

[40] C. L. Henley, Relaxation time for a dimer covering with height representation, J. Stat. Phys. **89**, 483 (1997).

[41] J. Cano and P. Fendley, Spin Hamiltonians with Resonating-Valence-Bond Ground States, Phys. Rev. Lett. **105**, 067205 (2010).

[42] M. Mambrini, S. Capponi, and F. Alet, Engineering SU(2) invariant spin models to mimic quantum dimer physics on the square lattice, Phys. Rev. B **92**, 134413 (2015).

[43] J. I. Cirac, D. Poilblanc, N. Schuch, and F. Verstraete, Entanglement spectrum and boundary theories with projected entangled-pair states, Phys. Rev. B **83**, 245134 (2011).

compute the entanglement entropy of the boundary state, provide the entanglement spectrum of the $\mathbb{Z}_2$ phase [43], and give the expression of the parent Hamiltonian at $\lambda = 0$ [41].